ISSN 1023-1935, Russian Journal of Electrochemistry, 2017, Vol. 53, No. 10, pp. 1087–1099. © Pleiades Publishing, Ltd., 2017.
Published in Russian in Elektrokhimiya, 2017, Vol. 53, No. 10, pp. 1225–1238.

Estimating Parameters from Rotating Ring Disc Electrode Measurements[1, 2]

Shriram Santhanagopalan[a] and Ralph E. White[b, *]

[a] *Transportation and Hydrogen Systems Center, National Renewable Energy Laboratory, Golden CO 80401, USA*
[b] *Department of Chemical Engineering, University of South Carolina, Columbia SC 29208, USA*
**e-mail: white@engr.sc.edu*

Received November 12, 2016; in final form, March 9, 2017

Abstract—Rotating ring disc electrode (RRDE) experiments are a classic tool for investigating kinetics of electrochemical reactions. Several standardized methods exist for extracting transport parameters and reaction rate constants using RRDE measurements. In this work, we compare some approximate solutions to the convective diffusion used popularly in the literature to a rigorous numerical solution of the Nernst–Planck equations coupled to the three dimensional flow problem. In light of these computational advancements, we explore design aspects of the RRDE that will help improve sensitivity of our parameter estimation procedure to experimental data. We use the oxygen reduction in acidic media involving three charge transfer reactions and a chemical reaction as an example, and identify ways to isolate reaction currents for the individual processes in order to accurately estimate the exchange current densities.

Keywords: rotating ring disc electrodes, hydrodynamics, simultaneous reactions, sensitivity analysis

DOI: 10.1134/S1023193517100111

INTRODUCTION

The rotating ring disk electrode (RRDE) is popular [1–5] in electrochemical studies both for its ease of use as well as for the rigor with which kinetic data can be obtained across a variety of operating conditions. The computational tools developed to simulate the setup also constitute one of the most rigorously studied systems in electrochemical engineering [6–10]. The fluid motion due to a rotating disk is described by the Navier–Stokes equations and the continuity equation. This system of equations can be simplified to a set of two-dimensional (2D) equations using the steady-state, the axial symmetry, and the incompressible Newtonian fluid assumptions [11, 12]. They are usually further reduced to a set of one-dimensional (1D) equations by a combination of variables technique as presented by von Kármán. [13] The 1D equations subject to a set of concise boundary conditions are then solved using a variety of techniques including series expansions [14–16] and numerical solutions [17, 18]. Modeling kinetics using the rotating disk electrode consists of solving the convective-diffusion equations that describe the rate of mass transport to the rotating disk surface. Exact analytical solution to this problem is only possible for relatively simple cases [19]. For more complicated cases, such as those involving multiple reactions taking place simultaneously at the electrode surface, researchers have often resorted to limiting case analyses [20–22] where the rates of one or more reactions are negligible under a limited potential or concentration window, or when the contribution of migration to charge transport is ignored [23]. Numerical solution techniques offer generic solutions; but are often tedious to develop. This is particularly true of non-linear differential algebraic systems such as electrochemical reactions coupled with convective flow [24–26] since the convergence of the numerical scheme depends to a large extent on the initial guess values. This problem is usually circumvented by solving the transient problem in successive iterations until steady-state conditions are arrived at. Solving directly for the steady state condition where the flow is fully developed and reaction equilibrium is established, results in a much more efficient solution scheme [27]. Following the model [7] developed by White and Newman to solve for the steady state conditions on a rotating disc electrode involving simultaneous reactions, Lorimer [28] and Adanuvor [29–31] presented extensions to include chemical reactions at the interface and in the bulk of the solution. The latter also presented a rigorous mathematical procedure to extract model parameters from a set of rotating disc electrode

[1] This paper is the author's contribution to the special issue of Russian Journal of Electrochemistry dedicated to the 100th anniversary of the birth of the outstanding Soviet electrochemist Veniamin G. Levich.
[2] The article is published in the original.

measurements. Simulating multiple reactions on a rotating ring disc electrode surface is complicated by the need to specify model parameters accurately, in addition to solving a highly non-linear set of equations that require a consistent set of initial conditions. In most instances, the kinetic and transport parameters are obtained by trial and error [30]. Even when a method to extract parameters from experimental data does exist, [31] there are practical difficulties such as discerning the contributions from competing factors. For instance, Wu et al. [32] use a frequency domain solution and observe dispersions at specific sets of frequencies that they attribute to formation of adsorbed intermediates or coupling between double layer charging and faradaic reactions. Other techniques such as transient measurements using rotating electrodes [33] or eccentric rotating electrodes [34] are often limited by constraints on experimental reproducibility of the flow fields.

More recently, rigorous numerical solutions for the three dimensional flow problem coupled with surface reactions have been presented [35, 36]. We recently compared errors introduced from adapting only the first term of the series expansion for the velocity profiles [37] and presented a rigorous numerical solution for the Navier–Stokes equations coupled with the three dimensional flow problem [38]. Despite the extensive number of systems analyzed and the availability of advanced computational tools, the methodology to obtain kinetic information from rotating electrode experiments has essentially remained unchanged over the last few decades. In this work, we build upon our recent work on the numerical solution of a system involving multiple reactions [38]. Using the approach presented earlier by Adanuvor and White [31] we explore alternate designs for the RRDE set up, where in the contributions from individual reactions can be better resolved using additional ring electrodes set to different voltages.

MODEL DEVELOPMENT

The model system used for illustrative purposes in this work is the reduction of oxygen in acidic media. The reactions involved are as follows:

$$O_2 + 4H^+ + 4e \rightleftarrows 2H_2O \qquad U_1^\theta = 1.229\ \text{V} \qquad \text{reaction 1},$$
$$O_2 + 2H^+ + 2e \rightleftarrows H_2O_2 \qquad U_2^\theta = 0.695\ \text{V} \qquad \text{reaction 2},$$
$$H_2O_2 + 2H^+ + 2e \rightleftarrows 2H_2O \qquad U_3^\theta = 1.763\ \text{V} \qquad \text{reaction 3},$$
$$H_2O_2 \rightleftarrows 1/2\,O_2 + H_2O \qquad \Delta G_{298}^0 = -103.08\ \text{kJ/mol} \qquad \text{reaction 4}.$$

The parameter U_1^θ represents the standard electrode potential for the charge transfer reaction '*j*'. All the potentials mentioned in this work are with respect to the standard hydrogen electrode. ΔG_{298}^0 is the standard Gibb's free energy change in the chemical reaction at 298 K in kJ/mol.

In this work, the hydrodynamics at an RRDE is solved with a two dimensional model in cylindrical coordinates, based on the Navier–Stokes equations [9]. The Nernst–Planck equation is used to simulate mass transport [11, 39]. All the basic transport terms, including diffusion, convection, and the migration term are retained in the Nernst–Planck equation to ensure accuracy. The equations used for the boundary conditions on the disk and the ring where the electrochemical reactions occur are based on the Butler–Volmer kinetics [28–30]. The simulations were carried out by using the commercial finite element software, COMSOL[3] MultiPhysics (COMSOL) [40]. The model equations subject to the assigned boundary conditions are solved and polarization curves are simulated for cases in which the reactions 1~4 occur to different extents.

[3] www.comsol.com.

A sketch of the cross-section of the RRDE and the simulation domain adjacent to the surface of the electrodes is shown in Fig. 1. The variable z is used to represent the axial coordinate for which the origin is set at the surface of the electrode. The radial coordinate is represented by r and its origin is set at the center of the disc electrode. In accordance with the observation by F.M. White [9] that the velocity changes are negligible when the dimensionless distance ζ is greater than 10 and by A. J. Bard et al. [3] that a region of 0 to 7.2 ζ in the axial direction should be used for material balance, we chose z = 0–0.12 cm as the simulation domain. Here, $\zeta = z\sqrt{\Omega/(\mu/\rho)}$, where Ω is the rotating speed of the electrode in rad/s, μ is the kinematic viscosity in mPa s, and ρ is the density of the electrolyte in g/cm^3. Numbers in italics in the schematic shown in Fig. 1 represent the boundaries as referenced in subsequent sections. The boundary *2* corresponds to the disc electrode; *5* and *7* are the two ring electrodes and their positions in the baseline case are as described in Fig. 1; *4, 6* and *8* are insulated boundaries representing the Teflon block on to which the electrodes are embedded; boundaries *2* and *9* have convective flux with no normal stresses. The pressure is set to zero at $r = z = 0$.

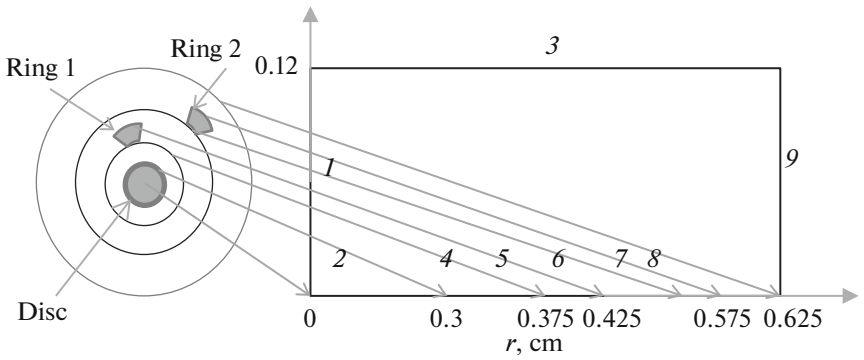

Fig. 1. Schematic of an RRDE and the modeling domain showing the two staggered ring electrodes. The numbers along the boundaries correspond to those listed on the first column of Table 2.

Momentum Balance (Swirl Flow Model)

The following assumptions are made in this model: the electrolyte is a Newtonian fluid with constant density and viscosity; the physical properties of the electrolyte (0.5 M H_2SO_4 saturated with pure oxygen at 1 atm and 298 K) can be approximated by those of water; the system has axial symmetry and is at steady state. The generalized equations of motion and continuity in cylindrical coordinates are in the following form [39]:

$$\rho\frac{\partial \mathbf{u}}{\partial t} - \nabla\cdot\mu\left(\nabla\mathbf{u} + (\nabla\mathbf{u})^T\right) + \rho(\mathbf{u}\cdot\nabla)\mathbf{u} + \nabla P = 0, \quad (1)$$

$$\nabla\cdot\mathbf{u} = 0, \quad (2)$$

where P is the pressure in Pa, $\mathbf{u}$ is the velocity vector in cm/s. With the assumption of axial symmetry and steady state flow, the derivatives with respect to time (t), and angular coordinate (θ) are all equal to zero. The density and viscosity are assumed to be constants. Eqs. (1) and (2) can then be simplified and written in the expanded form as shown in Table 1.

Mass Balance (Nernst–Planck Equations)

The following assumptions are made for the mass balance: the system is assumed to be at steady state; there are no homogeneous reactions in the bulk of the electrolyte; the axial symmetry condition is applicable; the concentrations and the liquid phase potential

Table 1. Santhanagopalan and White

	Expressions
Governing equations for velocity and pressure	$\frac{1}{r}\frac{\partial}{\partial r}(ru_r) + \frac{\partial}{\partial z}(u_z) = 0$ $\rho\left(u_r\frac{\partial u_r}{\partial r} - \frac{u_\theta^2}{r} + u_z\frac{\partial u_r}{\partial z}\right) = -\frac{\partial p}{\partial r} + \mu\left(\frac{1}{r}\frac{\partial}{\partial r}\left(r\frac{\partial u_r}{\partial r}\right) - \frac{u_r}{r^2} + \frac{\partial^2 u_r}{\partial z^2}\right)$ $\rho\left(u_r\frac{\partial u_\theta}{\partial r} + \frac{u_r u_\theta}{r} + u_z\frac{\partial u_\theta}{\partial z}\right) = \mu\left(\frac{1}{r}\frac{\partial}{\partial r}\left(r\frac{\partial u_\theta}{\partial r}\right) - \frac{u_\theta}{r^2} + \frac{\partial^2 u_\theta}{\partial z^2}\right)$ $\rho\left(u_r\frac{\partial u_z}{\partial r} + u_z\frac{\partial u_z}{\partial z}\right) = -\frac{\partial P}{\partial z} + \mu\left(\frac{1}{r}\frac{\partial}{\partial r}\left(r\frac{\partial u_z}{\partial r}\right) + \frac{\partial^2 u_z}{\partial z^2}\right)$
Governing equations for concentration and potential	$u_r\frac{\partial c_i}{\partial r} + u_z\frac{\partial c_i}{\partial z} = D_R\left(\frac{\partial^2 c_i}{\partial z^2} + \frac{\partial^2 c_i}{\partial r^2} + \frac{1}{r}\frac{\partial c_i}{\partial r}\right)$ $+ z_i\frac{D_i}{RT}F\left[c_i\left(\frac{\partial^2\Phi}{\partial z^2} + \frac{\partial^2\Phi}{\partial r^2} + \frac{1}{r}\frac{\partial\Phi}{\partial r}\right) + \left(\frac{\partial c_i}{\partial r} + \frac{\partial c_i}{\partial z}\right)\left(\frac{\partial\Phi}{\partial r} + \frac{\partial\Phi}{\partial z}\right)\right]$, where $i = 1, 2, 3, 4$ respect to HSO_4^-, H_2O_2, H^+ and O_2 $\sum_i z_i c_i = 0$

do not change at positions far away from the electrochemical reaction sites.

The general form of the Nernst–Planck equation used for the mass balance is as follows [21]:

$$\nabla \cdot \left(-D_i \nabla c_i - z_i c_i F \frac{D_i}{RT} \nabla \Phi + c_i \mathbf{u} \right) = 0, \quad (3)$$

where c_i is the concentration of species '*i*' in mol/cm^3 (i = 1, 2, 3 and 4 represent HSO_4^-, H_2O_2, H^+ and O_2, respectively), D_i is the diffusion coefficient of the species '*i*' in cm^2/s, z_i is the charge on species '*i*', F is Faraday's constant 96 486 C/mol [41] and Φ is the potential in the electrolyte in V. Equation 3 can be written for each species corresponding to i = 1, 2, 3, and 4; but there are 5 variables including 4 concentrations ($c_{1\sim4}$) and the potential in the liquid phase (Φ) that need to be solved for. In the calculation procedure, one of the concentrations (c_1, the concentration of HSO_4^-) is obtained from the electroneutrality condition:

$$\sum_{i=1}^{4} z_i c_i = 0, \quad (4)$$

and c_2, c_3, c_4 and Φ are solved with the 4 equations represented by equation 3.

Boundary Conditions for Velocity and Pressure

Boundary *1* (see Fig. 1) is at the axis of the cylindrical coordinate, and axial symmetry conditions are applicable.

$$u_r = 0, \; u_\theta = 0, \text{ at } r = 0, \; \forall z. \quad (5)$$

Boundary *9* is far away from the axis of the cylindrical coordinate, and is treated as free surfaces (i.e., the viscous force is zero):

$$\mu \left(\nabla \mathbf{u} + (\nabla \mathbf{u})^T \right) \cdot \mathbf{n} = 0 \text{ at } r = 0.75 \text{ cm}, \; \forall z, \quad (6)$$

or, in the expanded form:

$$\begin{gathered} -\mu \left(2 \frac{\partial u_r}{\partial r} \right) = 0, \; -\mu \left(r \frac{\partial}{\partial r} \left(\frac{u_\theta}{r} \right) \right) = 0, \\ -\mu \left(\frac{\partial u_r}{\partial z} + \frac{\partial u_z}{\partial r} \right) = 0, \text{ at } r = 0.75 \text{ cm}, \; \forall z. \end{gathered} \quad (7)$$

At the surface of the electrodes, the no-slip condition is assumed to apply, hence the r and z components of the velocity are set equal to zero, while the θ component of the velocity is set equal to the angular velocity of the electrode. So the velocities at boundaries *2, 4–8* are given by:

$$u_r = 0, u_z = 0 \text{ and } u_\theta = \Omega r \text{ at } z = 0, \; \forall r. \quad (8)$$

Only the first order derivative of the pressure (P) exists in the governing equation (1), which means that only one boundary condition in the z direction for pressure (P) is needed [39]. The pressure (P) is arbitrarily set to be zero at boundary *3*. The derivative of velocity in z direction is equal to zero since it has a constant value far from the surface of the electrode (i.e., along boundary *3*) [20, 21]. Also u_r and u_θ can be set equal to zero at boundary *3* since there is no viscous effect far from the electrode surface (except an axial inflow) [20]. So the following conditions for boundary *3* are given:

$$\begin{gathered} u_r = 0, \; u_\theta = 0, \; P = 0, \; \frac{\partial u_z}{\partial z} = 0, \\ \text{at } z = 0.12 \text{ cm}, \; \forall r. \end{gathered} \quad (9)$$

Boundary Conditions for Concentrations and Potential

Axial symmetry is used to set the boundary conditions at boundary *1*, which is located at r = 0:

$$\frac{\partial c_i}{\partial r} = 0, \; \frac{\partial \Phi}{\partial r} = 0 \text{ at } r = 0, \; \forall z. \quad (10)$$

The concentrations at boundary *3*, far away from the surface of the electrode, are the bulk concentrations ($c_{i,\text{ bulk}}$, in mol/cm^3), and the potential Φ is set equal to the potential of the reference electrode at the operating conditions (Φ_{RE}, in V).

$$c_i = c_{i,\text{bulk}}, \; \Phi = \Phi_{RE} \text{ at } z = 0.12 \text{ cm}, \; \forall r. \quad (11)$$

At boundaries *2*, *5* and *7* which are on the surface of the disk and the ring electrodes, reactions 1–4 occur, and a jump material balance gives the following [11, 31] equations:

$$\begin{gathered} \left[D_i \frac{dc_i}{dz} + z_i c_i F \frac{D_i}{RT} \frac{d\Phi}{dz} \right] = \sum_{j=1}^{3} \frac{s_{i,j} i_j}{n_j F} + s_{i,4} r_s \\ \text{for } i = 2, 3, 4; \\ F \sum_{i=1}^{4} z_i \left(-D_i \frac{dc_i}{dz} - z_i c_i F \frac{D_i}{RT} \frac{d\Phi}{dz} \right) = i_t \\ \text{at } \; r = 0 \sim 0.25 \text{ or } r = 0.325 \sim 0.375 \text{ cm}, \; z = 0, \end{gathered} \quad (12)$$

where s_{ij} is the stoichiometric coefficient of species '*i*' in reaction '*j*', i_j is the current density for reaction '*j*' in A/cm^2, i_t is the total current density in A/cm^2, n_j is the number of electrons transferred in reaction '*j*', r_s is the chemical reaction (i.e. reaction 4) rate at the electrode surface in mol/(cm^2 s), R is the gas constant, 8.314 J/(mol K), and T is the absolute temperature in K. In the first expression in equation (12), the left hand side is the mass flux of each species, and the right hand side is the generation or consumption of the respective species due to chemical and/or electrochemical reactions. In the second expression in equation (12), the left hand side is the net flux of charge in the electrolyte adjacent to the electrode surface, while the right hand side is the total current flow. At bound-

aries *4*, *6* and *8*, the current will be zero, since there are no reactions occurring:

$$0 = \left[D_i \frac{dc_i}{dz} + z_i c_i F \frac{D_i}{RT} \frac{d\Phi}{dz} \right] \text{ for } i = 2, 3, 4;$$
$$0 = \sum_{i=1}^{4} z_i \left(-D_i \frac{dc_i}{dz} - z_i c_i F \frac{D_i}{RT} \frac{d\Phi}{dz} \right) \quad (13)$$

at $r = 0.25 \sim 0.325$ or $r = 0.375 \sim 0.75$ cm, $z = 0$.

Boundary *9* is far away from the axis of the cylindrical coordinate, and following conditions are applied:

$$0 = \left[D_i \frac{dc_i}{dr} + z_i c_i F \frac{D_i}{RT} \frac{d\Phi}{dr} \right] \text{ for } i = 2, 3, 4;$$
$$0 = \sum_{i=1}^{4} z_i \left(-D_i \frac{dc_i}{dr} - z_i c_i F \frac{D_i}{RT} \frac{d\Phi}{dr} \right) \text{ at } r = 0.75, \ \forall z. \quad (14)$$

Note that z_i is equal to zero for neutral species O_2 and H_2O_2 ($i = 1$ and 2 respectively) in equations (12)–(14).

Kinetic Equations

The current densities in equation (12) can be obtained from the kinetic equations for the electrochemical reactions at the electrode surface based on the Butler–Volmer expression [25–27]:

$$i_j = i_{0j,\text{ref}} \left\{ \prod_i \left(\frac{c_{i,0}}{c_{i,\text{ref}}} \right)^{p_{i,j}} \exp\left(\frac{\alpha_{a,j} F}{RT} \eta_j \right) - \prod_i \left(\frac{c_{i,0}}{c_{i,\text{ref}}} \right)^{q_{i,j}} \exp\left(-\frac{\alpha_{c,j} F}{RT} \eta_j \right) \right\}, \quad (15)$$

where $i_{0j,\text{ref}}$ is the exchange current density due to reaction *'j'* at the reference concentrations in A/cm^2, $c_{i,0}$ is the concentration of species *'i'* adjacent to the surface of electrode in mol/cm^3, $c_{i,\text{ref}}$ is the reference concentration of species *'i'* in mol/cm^3, α_{aj} is the anodic transfer coefficient for reaction *'j'*, α_{cj} is the cathodic transfer coefficient for reaction *'j'*, p_{ij} is the anodic reaction order of species *'i'* in reaction *'j'*, q_{ij} is the cathodic reaction order of species *'i'* in reaction *'j'*, and η_j is the overpotential of reaction *'j'* in V, and it is measured with respect to a reference electrode of a given kind in a solution at the reference concentrations. The open circuit potential of reaction *'j'* at the reference concentrations relative to a standard reference electrode of a given kind is expressed [28] as follows:

$$U_{j,\text{ref}} = U_j^{\theta} - \frac{RT}{n_j F} \sum_i s_{i,j} \ln\left(\frac{c_{i,\text{ref}}}{\rho} \right) - U_{\text{RE}}^{\theta} + \frac{RT}{n_{\text{RE}} F} \sum_i s_{i,\text{RE}} \ln\left(\frac{c_{i,\text{RE}}}{\rho} \right), \quad (16)$$

where $s_{i,\text{RE}}$ is the stoichiometric coefficient of species *'i'* in the reaction occurring at the reference electrode, $U_{j,\text{ref}}$ is the open circuit potential of the reaction *'j'* at the reference concentrations relative to a standard reference electrode of a given kind in V, U_{RE}^{θ} is the potential of the standard reference electrode, $c_{i,\text{RE}}$ is the concentration of species *'i'* at the reference electrode in mol/cm^3, n_{RE} is the number of electrons transferred in the reaction that occurs at the reference electrode. The overpotential for electrochemical reaction *'j'*, (η_j) in equation (15) is given by

$$\eta_j = \Phi_{\text{met}} - \Phi_{\text{RE}} - (\Phi_0 - \Phi_{\text{RE}}) - U_{j,\text{ref}}, \quad (17)$$

where Φ_0 is the potential in the solution adjacent to the electrode surface in V, Φ_{met} is the potential of working electrode in V. The reaction orders $p_{i,j}$ and $q_{i,j}$ in equation 15 are related to $s_{i,j}$ by

$$p_{i,j} = s_{i,j} \quad q_{i,j} = 0 \quad \text{if} \quad s_{i,j} > 0, \quad (18)$$

$$p_{i,j} = 0 \quad q_{i,j} = -s_{i,j} \quad \text{if} \quad s_{i,j} > 0. \quad (19)$$

The apparent transfer coefficients for reaction *'j'* sum up to the number of electrons transferred in that reaction, that is

$$\alpha_{a,j} + \alpha_{c,j} = n_j. \quad (20)$$

The total current density is the sum of the partial current densities

$$i_t = \sum_{j=1}^{3} i_j. \quad (21)$$

The rate of the catalytic decomposition of peroxide at the electrode surface is expressed as

$$r_s = -k_h c_{\text{H}_2\text{O}_2,0}^{p}, \quad (22)$$

where the reaction order (p) can be a fraction or a whole number, and it is assumed to be 1 in this work. One of the key differences in the system described in Fig. 1, from experimental set-up previously described (see for example [37, 38]) is the ability to independently control the applied potential (E_{appl}, or $\Phi_{\text{met}} - \Phi_{\text{RE}}$) at the surface of each of the ring electrodes. As noted in subsequent sections, this feature significantly enhances the sensitivity of the i–V data to the kinetic parameters associated with the individual reactions. The rate constant k_h is assumed to be independent of the applied potential. Summaries of the governing equations and the boundary conditions (including the kinetic equations) are listed in Tables 1 and 2, respectively. The governing equations (equations (1)–(4)) subject to the given boundary conditions (equations (5)–(22)) are solved numerically using COMSOL. The kinetic parameters, reaction properties and physical properties of the species used in this simulation are shown in Table 3. The values for other system invariants, solution phase properties and the operating conditions are listed in Table 4.

Table 2. Santhanagopalan and White

Boundary *1*	$u_r = 0, u_\theta = 0,$ at $r = 0,$ all z
Boundary *9*	$-\mu\left(2\frac{\partial u_r}{\partial r}\right) = 0, \ -\mu\left(r\frac{\partial}{\partial r}\left(\frac{u_\theta}{r}\right)\right) = 0,$ $-\mu\left(\frac{\partial u_r}{\partial z} + \frac{\partial u_z}{\partial r}\right) = 0,$ at $r = 0.75$ cm, $\forall\, z$
Boundaries *2, 4–8*	$u_r = 0, u_z = 0, u_\theta = \Omega r,$ at $z = 0,$ all r
Boundary *3*	$u_r = 0, u_\theta = 0, \ P = 0$ at $z = 0.12$ cm for all r
Boundary *1*	$\frac{\partial c_i}{\partial r} = 0, \ \frac{\partial \Phi}{\partial r} = 0$ at $r = 0,$ all z
Boundary *3*	$c_i = c_{i,\text{bulk}}, \Phi = \Phi_{\text{re}}$ at $z = 0.12$ cm, all r
Boundaries *2, 5* and *7*	$\sum_{j=1}^{3}\frac{s_{i,j}i_j}{n_jF} + s_{i,4}r_s = \left[D_i\frac{dc_i}{dz} + z_ic_iF\frac{D_i}{RT}\frac{d\Phi}{dz}\right]$ for $i = 2, 3, 4$ $i_t = F\sum_{i=1}^{4}z_i\left(-D_i\frac{dc_i}{dz} - z_ic_iF\frac{D_i}{RT}\frac{d\Phi}{dz}\right)$ at $r = 0 \sim 0.25$ or $r = 0.325 \sim 0.375$ cm, $z = 0$
Boundaries *4, 6* and *8*	$0 = \left[D_i\frac{dc_i}{dz} + z_ic_iF\frac{D_i}{RT}\frac{d\Phi}{dz}\right]$ for $i = 2, 3, 4$ $0 = \sum_{i=1}^{4}z_i\left(D_i\frac{dc_i}{dz} + z_ic_iF\frac{D_i}{RT}\frac{d\Phi}{dz}\right)$ at $r = 0.25 \sim 0.325$ or $r = 0.375 \sim 0.75$ cm, $z = 0$
Boundary *9*	$0 = \left[D_i\frac{dc_i}{dr} + z_ic_iF\frac{D_i}{RT}\frac{d\Phi}{dr}\right]$ for i=2,3,4 $0 = \sum_{i=1}^{4}z_i\left(-D_i\frac{dc_i}{dr} - z_ic_iF\frac{D_i}{RT}\frac{d\Phi}{dr}\right)$ at $r = 0.75, \ \forall$ z
Butler–Volmer equation	$i_j = i_{0j,\text{ref}}\left\{\prod_i\left(\frac{c_{i,0}}{c_{i,ref}}\right)^{p_{i,j}}\exp\left(\frac{\alpha_{a,j}F}{RT}\eta_j\right) - \prod_i\left(\frac{c_{i,0}}{c_{i,\text{ref}}}\right)^{q_{i,j}}\exp\left(-\frac{\alpha_{c,j}F}{RT}\eta_j\right)\right\}$
Overpotential	$\eta_j = \Phi_{\text{met}} - \Phi_{\text{RE}} - (\Phi_0 - \Phi_{\text{RE}}) - U_{j,\text{ref}}$
Reference electrode potential	$U_{j,\text{ref}} = U_j^\theta - \frac{RT}{n_jF}\sum_i s_{i,j}\ln\left(\frac{c_{i,\text{ref}}}{\rho}\right) - U_{RE}^\theta + \frac{RT}{n_{\text{RE}}F}\sum_i s_{i,\text{RE}}\ln\left(\frac{c_{i,\text{RE}}}{\rho}\right)$
Reaction orders	$\begin{cases} p_{i,j} = s_{i,j} \quad q_{i,j} = 0 \quad \text{if} \quad s_{i,j} > 0 \\ p_{i,j} = 0 \quad q_{i,j} = -s_{i,j} \quad \text{if} \quad s_{i,j} < 0 \end{cases}$
Chemical reaction (reaction 4)	$r_s = -k_{fl}c_{H_2O_2,0}^p$

SENSITIVITY ANALYSIS

It is common practice to design experiments such that the change in the response is sufficiently sensitive to model parameters of interest. In this instance, we are primarily interested in calibrating the current-voltage response of the RRDE system and regressing the exchange current densities or transfer coefficients from the fits. As shown in the following section, this process is straight-forward for single reactions. However, with an increase in the number of reactions taking place simultaneously, it is desirable to perform a sensitivity analysis a priori, to screen the parameter space for maximum resolution in the sensitivity coefficients. A detailed procedure to perform such analyses was outlined by Adanuvor [31]. For a system of equations with a parameter set **x**, the objective function (F)

Table 3. Santhanagopalan and White

Kinetic parameters	Reaction 1	Reaction 2	Reaction 3	Reaction 4
α_{cj}	1.0	0.8–1.2	0.25–0.45	
$i_{0,\mathrm{ref}}$ (A/cm^2)	10^{-9}	10^{-4}~10^{-9}	10^{-15}~10^{-19}	
U_j^{θ} (V) [9]	1.229	0.695	1.736	
n_j	4	2	2	
k_h mol/s (mol/cm^3)				10^{-1}~10^{0}
P				1
Reaction properties	HSO_4^-	H_2O_2	H^+	O_2
$s_{i,1}$	0	0	–4	–1
$s_{i,2}$	0	+1	–2	–1
$s_{i,3}$	0	–1	–2	0
$s_{i,4}$	0	1	0	–0.5
Z	–1	0	+1	0
Solution properties	HSO_4^-	H_2O_2	H^+	O_2
$c_{i,\mathrm{ref}}$ (mol/cm^3)	0.00051	1.377×10^{-14}	0.0005	0.13×10^{-6}
D_i (cm^2/s) [21, 33]	1.33×10^{-5}	1.16×10^{-5}	9.312×10^{-5}	1.79×10^{-5}

to minimize the error between the model predictions and experimental observations is given by:

$$F(\mathbf{x},t) = \sum_{k=1}^{n} w_k \left(y_{k,\mathrm{expt}} - f(\mathbf{x},t)\right)^2. \quad (23)$$

The vector of parameters is then iteratively updated using the following expression:

$$\mathbf{x}^{j+1} = \mathbf{x}^j + \mathbf{\Delta x}^j, \quad (24)$$

where $\mathbf{\Delta x}^j$ is calculated as the gradient on the parameter space that minimizes the objective function. For second order methods using the Hessian (**H**) of the objective function, the following definitions apply:

$$\mathbf{\Delta x}^j = \left[\mathbf{H}^j\right]^{-1} \mathbf{q}^j, \quad (25)$$

$$\mathbf{H}^j_{\alpha\beta} = 2\sum_{k=1}^{n} w_k^j \frac{\partial f_k^j}{\partial x_\alpha}\frac{\partial f_k^j}{\partial x_\beta}, \quad (26)$$

$$q_\alpha^j = \frac{\partial F^j}{\partial x_\alpha}. \quad (27)$$

Here, q_α^j is the sensitivity coefficient and is a measure of how accurately one can determine the parameter x_α using the data point F^j. Our objective then, is to selectively improve the sensitivity of the current–voltage curves to the desired subset of parameters, in the presence of multiple reactions on the electrode surface, by exploring alternate experimental conditions. For ease of comparison against different test cases, we follow the convention introduced by Adanuvor [31] and define a relative sensitivity ($\bar{q}_\alpha^j$) as follows:

$$\bar{q}_\alpha^j = \left|\left(\frac{x_\alpha}{F^j}\right)\left(\frac{1}{q_\alpha^j}\right)\right|, \quad (28)$$

which helps us to identify the dominant set of parameters that influence the response under a given set of experimental conditions.

RESULTS AND DISCUSSION

Figure 2a shows the velocity field vector in the electrolyte as a function of distance from the electrode surface. The simulation captures features of the swirl flow, where in the electrolyte moves from the bulk

Table 4. Santhanagopalan and White

F	96 486 C/mol
R	8.314 J/(K mol)
T	298.15 K
U_{RE}^{θ}	0 V
ρ_0	0.001 kg/cm^3
N	0.012 cm^2/s
Ω	900 rpm
Applied potential on ring 1	1.2 V
Applied potential on ring 2	0.2–1.2 V

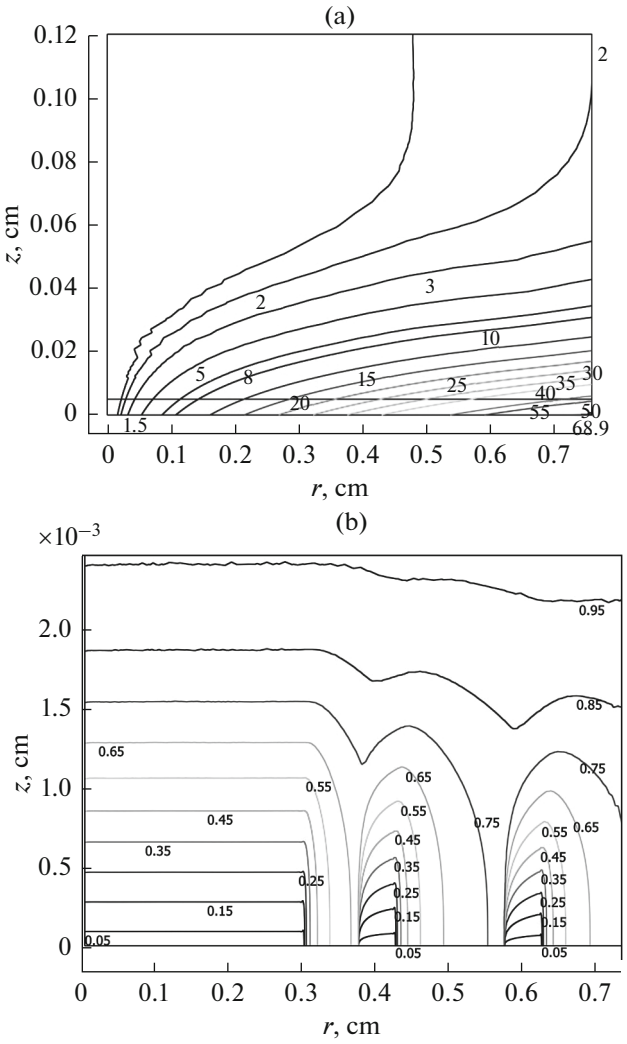

Fig. 2. Simulation of the three dimensional convective diffusion equations: (a) the velocity vector captures the features of the swirl flow accurately; (b) changes in the dimensionless concentration of the species in the electrolyte participating in the reactions at the electrode surface are limited to a small distance from the interface.

towards the surface and then in the radial direction away from $r = 0$. The velocity of the electrolyte is at its maximum on the outer edge of the rotating disc. The maximum velocity (=70.68 m/s) at boundary 7 where $u_r = u_z = 0$, corresponds to the rotation speed of 900 rpm. Figure 2b shows the distribution of the dimensionless concentration for the species of interest adjacent to the electrode surface. As noted, the concentration reaches the bulk values within a few microns from the electrode surface. Positioning the disc and ring electrodes at different levels along the z coordinate, it is numerically possible to solve for current distributions. However, the narrow reaction zone implies that using such an alternate design it is not practically viable to improve accuracy of the parameters estimated from such experimental data, since it

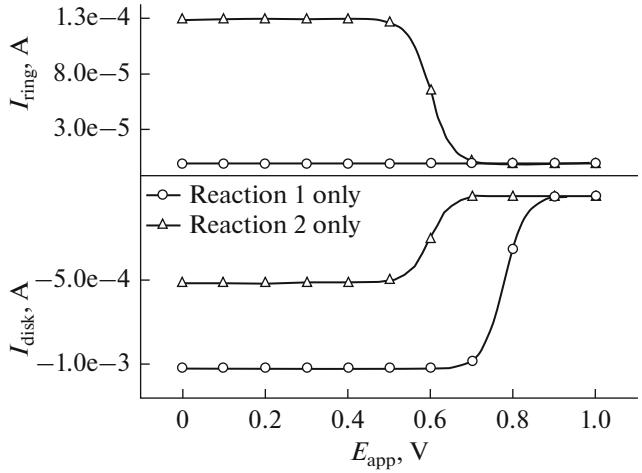

Fig. 3. Ring and Disc currents for competing reactions 1 and 2 when each reaction is hypothetically treated as the only one in progress: for this case the bias voltage on both the ring electrodes was set to 1.2 V. In theory, studying the reactions one at a time facilitates the estimation of kinetic properties; in practice, it is difficult to identify the observable sample space when multiple reactions take place at the electrode surface.

would be extremely difficult to precisely machine the differences in height between the ring and the disc electrodes.

Next, we simulate the current-voltage response for the individual reactions (1) and (2) to verify that the profiles are reasonable. In order to compare our results against previous work, we hold the potentials on both the ring electrodes at 1.2 V. Reaction 1 is the fundamental reaction of the ORR at an RRDE in an acidic electrolyte, and it can be used to simulate the experimentally obtained polarization curves approximately. The solid lines marked with open circles in Fig. 3 are simulation results for reaction 1 only with parameters $i_{0,1} = 10^{-9}$ A/cm^2 and $\alpha_{c1} = 1$. There is no current on the ring since there is no peroxide generated. The curve for disk current follows the trends for that of single reaction systems [27]. This result implies that the polarization curve shifts towards more cathodic potentials if $i_{0,1}$ gets smaller as the overall reaction rate is slower. On the other hand, when $i_{0,1}$ is increased, it shifts towards more anodic potentials. The potential drop in the ohmic region will be drastic when the transfer coefficient (α_{c1}) is large, and the drop is mild when α_{c1} is small.

In cases where peroxide is a stable product, reaction (2) can be used to simulate the polarization curves. A set of simulated polarization curves for reaction (2) are shown in Fig. 3 and are represented by lines marked with triangles. The current gathered on the ring is positive due to the anodic reaction and the current gathered on the disk is negative due to the cathodic reaction. Reaction 2 is reversible under

the given operating conditions. The oxygen transferred to the disk surface is reduced to peroxide at a rate depending on the applied potential (E_{appl}) and the mass transfer limitations. When the peroxide is transferred to the ring on which a constant potential of 1.2 V is applied, it is oxidized back to oxygen. The collection efficiency N of an RRDE is defined by:

$$N = \frac{I_R}{I_D}, \quad (29)$$

where I_R is the limiting current collected on the ring in A, I_D is the limiting current collected on the disk in A, when a single reversible reaction is occurring on the disk and all the product collected on the ring can be converted back to the reactant. The value of N for the RRDE with dimensions shown in Fig. 1 obtained using the analytical calculation method developed by W.J. Albery et al. is 0.24 [10, 41]. The value of N obtained in the simulation for reaction 2 only in this work is 0.25. The experimental result published by Markovic et al. was 0.23 [42]. These values for N are in good agreement. The limiting current predicted by Levich equation [1]

$$I_L = 0.620nFAD_{O_2}^{2/3}\omega^{1/2}\nu^{-1/6}c_{O_2 bulk}, \quad (30)$$

is -5.32×10^{-4} A. However, the limiting current obtained in this simulation work is -5.15×10^{-4} A. The discrepancy arises from the truncated series solutions for the velocities [10] (of the order of z^3 for u_z and of z^2 for u_r) used in deriving the Levich equation. We previously reported [37] that the complete numerical solution improves the estimates for the limiting currents and collection efficiencies by as much as 4% compared to the one-term approximation commonly used in the literature. The velocity profile obtained in this work using the swirl flow model is consistent with the numerical solution of the 1 dimensional model given by F.M. White [9]. We also verified that the simulations using truncated series solutions for the velocities and the Nernst–Planck equation for material balance result in the same limiting current value as the Levich equation prediction (i.e. $I_L = -5.32 \times 10^{-4}$ A).

Figure 4 shows the polarization curves when multiple reactions take place simultaneously at the electrode surface. The bias voltage for the ring electrodes was set to 1.0 V. The results from multiple reactions taking place on the electrode surface for a variety of conditions were discussed at length in our previous work [37, 38] and are not repeated here. It is worth noting that whereas in simulations it is possible to isolate the response of individual reactions by selectively setting the rate constants for all the other reactions to arbitrarily small values, in order to study the effect of different parameters on individual reactions, it is not often possible to obtain corresponding experimental data under such ideal conditions. For example, if reaction (4) takes place in the bulk, then the material balance equation shown in Table 1 would be modified as follows:

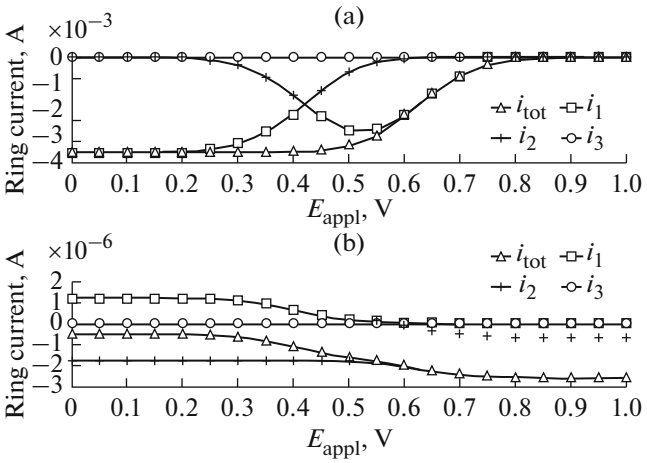

Fig. 4. Polarization curves for the case where competing reactions 1, 2, 3 and 4 all take place simultaneously. The contributions of reactions 1, 2 and 3 to the total current are shown. Reaction 4 is treated as a chemical reaction that takes place in the bulk. In this baseline case, the bias voltages for both the ring electrodes were set to 1.0 V.

$$u_r\frac{\partial c_i}{\partial r} + u_z\frac{\partial c_i}{\partial z} = D_R\left(\frac{\partial^2 c_i}{\partial z^2} + \frac{\partial^2 c_i}{\partial r^2} + \frac{1}{r}\frac{\partial c_i}{\partial r}\right) + \frac{z_i D_i F}{RT}\left[\left(\frac{\partial^2\Phi}{\partial z^2} + \frac{\partial^2\Phi}{\partial r^2} + \frac{1}{r}\frac{\partial\Phi}{\partial r}\right)c_i + \left(\frac{\partial c_i}{\partial r} + \frac{\partial c_i}{\partial z}\right)\left(\frac{\partial\Phi}{\partial r} + \frac{\partial\Phi}{\partial z}\right)\right] + R. \quad (31)$$

In such instances, it is beneficial to design experimental conditions in such a way as to maximize the relative sensitivity ($\overline{q}_\alpha^j$). One approach to alter the sensitivity of the different reactions would be to monitor the current distribution across different lengths from the disc [10]. However, given that the small variation in the solution phase potential, good conductivity across the ring electrodes, enhancements to the sensitivity of the reaction parameters will be minimal. In addition to this, the criteria for positioning the electrodes would be system specific, necessitating the use of a different set up for each parameter being identified, even within the same system. In our case, the wide differences in the standard electrode potentials offer an alternate option. We employ a segregated electrode similar to that proposed by Smyrl [10]; and in addition to the spatial isolation of the two ring electrodes, also employ different bias voltages ($\Phi_{met} - \Phi_{RE}$) for the ring electrodes. The numerical values for these voltages are selected based on the choice of parameters to be estimated. The simplest case is where the bias voltage is set equal to $U_{j,ref}$ when the current contribution for reaction j becomes zero. Thus, we can isolate the individual reaction currents at different ring electrodes.

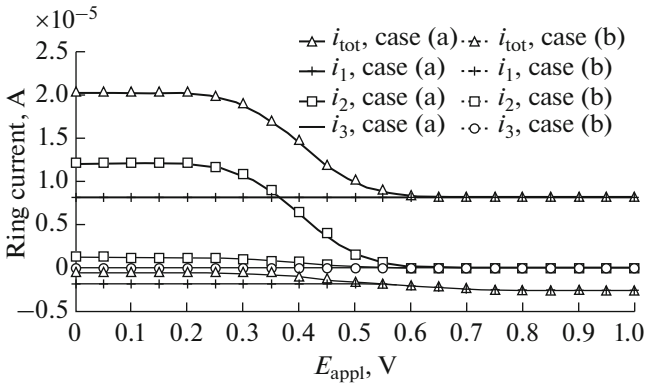

Fig. 5. Comparison of currents on the ring electrodes when (a) the bias voltage on the outer ring electrode was set to 1.2 V while retaining that on the inner ring electrode at 1.0 V (b) when the bias voltages were both set equal to 1.0 V (similar to the baseline case shown in Fig. 4).

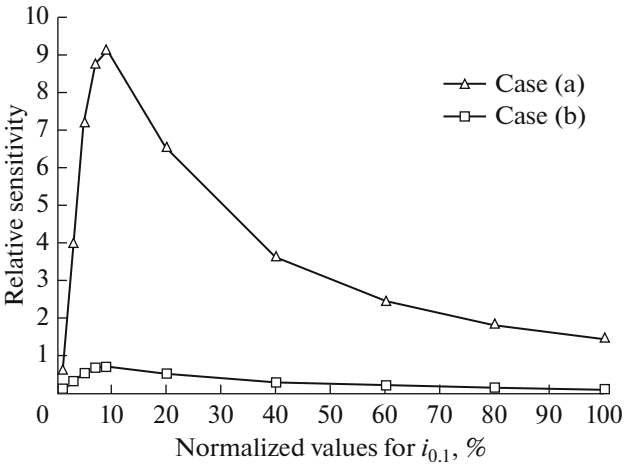

Fig. 6. Plots of the relative sensitivities for the reaction rate constant $i_{0,1}$ for different bias voltages corresponding to the cases shown in Fig. 5: Case (a) with the bias voltage on the ring electrodes equal to 1.0 and 1.2 V respectively and Case (b) with both the bias voltages set equal to 1.0 V.

Setting the voltage at the outer ring to more positive values compared to that at the inner ring selectively moves the current response for that reaction, whose standard electrode potential (U_j^θ) is closest to the bias voltage applied, to more cathodic values, providing a wider range of current–voltage curves that can be used to extract kinetic parameters for that reaction with higher fidelity.

One example of improving selectivity of the reaction currents is provided in Fig. 5. There are two sets of curves showing the ring currents. Those for case (b) were generated with the same set of parameters used in Fig. 4. The currents corresponding to case (a) were generated with 1.0 V for the bias voltage on the outer ring and 1.2 V for that on the inner ring electrode. As observed, the ring currents are enhanced by at least an order of magnitude. Similar results can be accomplished by sweeping the bias potential of an RRDE with one ring electrode across suitable values; however, the advantage of the segregated electrodes approach is the ability to isolate the individual reaction rates. For instance the bias voltage on the outer ring electrode can be set equal to $U_{1,\mathrm{ref}}$ and the reaction current for reaction (2) can be recovered with the same accuracy as those shown for case (b). Several other combinations of the bias voltages will facilitate extraction of parameters for other reactions.

One advantage of using the rigorous numerical solution presented in this work, is the ability to simulate potential and current distributions from multiple reactions across different electrodes, which enhances our ability to design experiments with features to sweep the bias voltages across suitable voltage windows. The downside is the large set of variables that need to be subjected through the design of experiments by trial and error. The estimation of sensitivity coefficients for the parameters of interest helps us narrow down the design space in a systematic fashion. Using the technique outlined in the previous sections, it is possible to obtain the relative sensitivity of the different parameters across the design space. The sensitivity coefficients can be calculated using analytical jacobians as part of the simulations in Comsol. Thus, knowing only the thermodynamic parameters for the system (viz., U_j^θ) and the bulk concentrations (which also equal the reference concentrations, in our simulations) for the species of interest, one can identify the design space suitable for estimating the rate constants for the different reactions that take place on the ring electrodes. Figure 6 shows the relative sensitivity of the exchange current densities obtained at different bias voltages. The range of parameter values chosen for the abscissa of the plot is still based on the initial estimates from the case where the potentials on the two ring electrodes are identical. By introducing bias voltages similar to those in Fig. 5, the sensitivity of the i–V curves to the parameter $i_{0,1}$ is improved considerably.

The modeling approach presented above can be used in conjunction with a variety of different mechanisms for electrode such as the Volmer–Tafel [28], Volmer–Heyrovsky [44], or Marcus–Hush–Chidsey (MHC). For diffusional redox systems, similar to the one presented in this work, the Butler–Volmer kinetics was reported to be more appropriate [45] to parameterize experimental data from voltammetric techniques. The MHC approach may provide additional physical insights; but its quantitative application is limited by the presence of additional parameters and has been shown to result in poor-quality fits of experimental data [45]. Determining kinetic parameters as outlined in the present work, the associated confidence intervals using the methodology presented in

[31] and conducting a statistical *t*-test to ascertain suitability of one of these mechanisms versus others, is a reasonable approach to studying kinetics of multiple reactions taking place simultaneously on an electrode surface.

CONCLUSIONS

The RRDE is a powerful and one of the most widely used tools for obtaining mechanistic information on electrochemical systems. With the availability of sophisticated computational tools, we are now able to simulate the flow problem in realistic geometries and probe a larger design space comprising of multiple parameters that influence the kinetics of oxygen reduction. Some quantitative metrics on improvements to the value of limiting currents predicted using the Levich equation that uses approximate solutions for the velocity profiles versus those calculated using the rigorous numerical models were discussed. We highlighted the use of a rigorous numerical model that solves for the flow and mass transport equations alongside the kinetics for a system where multiple reactions take place simultaneously on different electrode surfaces, and presented analytical tools for design of the RRDE system to maximize the sensitivity of the current-voltage curves to the parameters of interest.

LIST OF SYMBOLS

A	area of the disk, cm^2
c_i	concentration of species *'i'* (i =1, 2, 3, and 4 represent HSO_4^-, H_2O_2, H^+, and O_2, respectively), mol/cm^3
$c_{i,0}$	concentration of species *'i'* at the surface of the electrode, mol/cm^3
$c_{i,\ \mathrm{bulk}}$	concentration of species *'i'* in the bulk solution, mol/cm^3
$c_{i,\mathrm{ref}}$	reference concentration of species *'i'*, mol/cm^3
$c_{i,\mathrm{RE}}$	concentration of species *'i'* at the reference electrode, mol/cm^3
D_i	diffusion coefficient of species *'i'*, cm^2/s
F	Faraday's constant, 96 487 C/equiv
$i_{0j,\mathrm{ref}}$	exchange current density for reaction *'j'* at the reference concentrations, A/cm^2
$i_{0j,\mathrm{data}}$	exchange current density for reaction *'j'* at the reference concentrations, A/cm^2
I_L	limiting current calculated using the Levich equation, A
I_R	limiting current collected on the ring, A
I_D	limiting current collected on the disk, A
I_j	current generated by the reaction *'j'*, A
I_disk	current on the disk, A
I_ring	current on the ring, A
i_t	total current density defined in the 25, A/cm^2
i_j	current density of the reaction *'j'*, A/cm^2
k_h	rate constant for the chemical reaction (i.e. reaction (4)) at the electrode surface, mol/s (mol/cm^3)
n_j	stoichiometric number of electrons involved in the electrode reaction *'j'*
n_RE	stoichiometric number of electrons involved in the reaction that occurs at the reference electrode
N	collection efficiency of an RRDE
P	pressure in the electrolyte, Pa
p	reaction order of the reaction with no charge transfer (i.e., reaction (4))
p_{ij}	anodic reaction order of species *'i'* in reaction *'j'*
q_{ij}	cathodic reaction order of species *'i'* in reaction *'j'*
r	radial distance from the axis of the disk, cm
r_s	rate of chemical reaction (i.e., reaction (4)) at electrode surface, mol/cm^2 s
R	gas constant, 8.314 J/mol K
$s_{i,j}$	stoichiometric coefficient of species *'i'* in the reaction *'j'*
$s_{i,\mathrm{RE}}$	stoichiometric coefficient of species *'i'* in the reaction at the reference electrode
T	absolute temperature, K
u_r	radial component of the velocity, cm/s
u_z	axial component of the velocity, cm/s
u_θ	angular component of the velocity, cm/s
$s_{i,\mathrm{RE}}$	stoichiometric coefficient of species *'i'* in the reaction at reference electrode
U_j^θ	standard electrode potential for the charge transfer reaction *'j'*, V
$U_{j,\mathrm{ref}}$	open circuit potential of the reaction *'j'* at the reference concentrations relative to the reference electrode, V
U_RE^θ	standard potential of the reference electrode relative to SHE, V
$\mathbf{u}$	velocity vector, cm/s
z	axial distance, cm
$z_{\infty,v}$	axial distance considered to be sufficiently far from the electrode surface to be considered to be at "infinity" in the domain for the momentum balance, cm
$z_{\infty,m}$	axial distance considered to be sufficiently far from the electrode surface to be consid-

ered to be at "infinity" in the domain for material balance, cm

z_i charge on species *'i'*

Greek Symbols

$\alpha_{a,j}$ anodic transfer coefficient for reaction *'j'*

$\alpha_{c,j}$ cathodic transfer coefficient for reaction *'j'*

θ angular coordinate, rad

ρ density of the electrolyte, g/cm^3

μ kinematic viscosity of the electrolyte, mPa s

Φ potential in solution phase, V

Φ_0 potential in the solution adjacent to the electrode surface, V

Φ_{RE} potential of the reference electrode at the experimental conditions, V

Φ_{met} potential of the working electrode, V

Φ_{re} potential of the reference electrode at the experimental conditions, V

Ω rotating speed of the electrode, rad/s

η_j overpotential of reaction *'j'* corrected for ohmic drop in the solution and measured with respect to a reference electrode of a given kind in a solution at the reference concentrations, V

ΔG^0_{298} standard Gibbs free energy change in a chemical process at 298 K, kJ/mol

Subscripts

i species index, $i = 1$, 2, 3, and 4 represent HSO_4^-, H_2O_2, H^+, and O_2, respectively

j reaction index, $j = 1$, 2, and 3 correspond to reaction 1, 2, and 3, respectively

bulk properties or variables evaluated at the bulk solution

expt experimentally measured value

REFERENCES

1. Levich, V.G., *Physicochemical Hydrodynamics, Prentice Hall*, 1962, ISBN-13: 978-0136744405.
2. Compton, R.G., and Banks, C.E., *Understanding Voltammetry*, Imperial College Press, 2011, ISBN-13 978-1-84816-585-4.
3. Bard, A.J. and Faulkner, L.R., *Electrochemical Methods: Fundamentals and Applications*, John Wiley & Sons, *Inc.*, 2000, ISBN-13: 978-0471043720.
4. Gabe, D.R. and Walsh, F.C., *J. Appl. Electrochem.*, 1983, vol. 13, no. 1, pp. 3–21.
5. Tarasevich, M.R., Sadkowski, A., and Yeager, E., Kinetics and mechanisms of electrode processes, in *Comprehensive Treatise of Electrochemistry*, Horsman, P., Conway, B.E., and Yeager, E., Eds., New York: Plenum Press, 1983, vol. 7, p. 354.
6. Newman, J.S., *J. Phys. Chem.*, 1966, vol. 70, no. 4, pp. 1327–1328.
7. White, R.E. and Newman, J.S., *J. Electroanal. Chem.*, 1977, vol. 82, pp. 173–186.
8. Tribollet, B. and Newman, J.S., *J. Electrochem. Soc.*, 1983, vol. 130, pp. 2016–2026.
9. White, F.M., *Viscous Fluid Flow*, New York: McGraw-Hill, Inc, 1974.
10. Smyrl, W.H. and Newman, J.S., *J. Electrochem. Soc.*, 1972, vol. 119, pp. 212–219.
11. Newman, J. and Thomas-Alyea, K.E., *Electrochemical Systems*, 3rd Ed., New Jersey: John Wiley & Sons, Inc., 2004.
12. White, R.E., Mohr, C.M., Jr., and Newman, J., *J. Electrochem. Soc.*, 1976, vol. 123, p. 383.
13. v. Kármán, T. and Angew, Z., *Math. Mech.*, 1921, vol. 1, p. 486.
14. Cochran, W.G., *Proc. Cambridge Philos. Soc.*, 1934, vol. 30, p. 365.
15. Krylov, V.S. and Babak, V.N., *Sov. Electrochem.*, 1971, vol. 7, p. 826.
16. Nicancioglu, K. and Newman, J.S., *J. Electrochem. Soc.*, 1973, vol. 120, pp. 1356–1358.
17. Santhanagopalan, S. and White, R.E., *J. Electrochem. Soc.*, 2004, vol. 151, no. 8, pp. J50–J53.
18. Deslouis, C., Tribollet, B., Duprat, M., and Moran, F., *J. Electrochem. Soc.*, 1987, vol. 134, p. 2496.
19. Orazem, M.E., in *Tutorial: Application of Mathematical Models for Interpretation of Impedance Spectra*, Savinell, R.F., West, A.C., Renton, J.M., and Weidner, J., Ed., *The Electrochemical Society Proceedings Series*, NJ: Pennington, 1999, PV 99-14, p. 68.
20. Verbrugge, M.W., *J. Electrochem. Soc.*, 1992, vol. 139, p. 3529.
21. Pleskov, Yu.V. and Filinovskii, V.Yu., *The Rotating Disc Electrode*, New York: Consultants Bureau, 1976.
22. Beran, P. and Bruckenstein, S., *J. Phys. Chem.*, 1968, vol. 72, p. 3630.
23. White, R.E., Lorimer, S.E., and Darby, R., *J. Electrochem. Soc.*, 1983, vol. 130, no. 5, pp. 1123–1126.
24. Pons, S., *Electroanalytical Chemistry*, vol. 13, Bard, A.J., Ed., New York: Marcel Dekker, Inc., 1984.
25. Hale, J.M., *J. Electroanal. Chem. Interfacial Electrochem.*, 1964, vol. 8, p. 332.
26. Prater, K.B. and Bard, A.J., *J. Electrochem. Soc.*, 1970, vol. 117, p. 207.
27. Eddowes, M.J. and Grazel, M., *J. Electroanal. Chem. Interfacial Electrochem.*, 1983, vol. 152, p. 143.
28. White, R.E. and Lorimer, S.E., *J. Electrochem. Soc.*, 1983, vol. 130, no. 5, pp. 1096–1103.
29. Adanuvor, P.K., White, R.E., Lorimer, S.E., *J. Electrochem. Soc.*, 1987, vol. 134, no. 3, pp. 625–631.
30. Adanuvor, P.K. and White, R.E., *J. Electrochem. Soc.*, 1987, vol. 134, pp. 1093–1098.
31. Adanuvor, P.K. and White, R.E., *J. Electrochem. Soc.*, 1987, vol. 135, no. 8, pp. 1887–1898.
32. Wu, S-L., Orazem, M.E., Tribollet, B., and Vivier, V., *J. Electroanal. Chem.*, 2015, vol. 737, pp. 11–22.
33. Schmachtel, S. and Kontturi, K., *Electrochim. Acta*, 2011, vol. 56, no. 19, pp. 6812–6823.

34. Mohr, C.M., Jr. and Newman, J., *J. Electrochem. Soc.*, 1975, vol. 122, pp. 928–931.

35. Low, C.T.J., Roberts, E.P.L., and Walsh, F.C., *Electrochim. Acta*, 2007, vol. 52, p. 3833.

36. Tong, L., *Int. J. Surf. Eng. Coatings*, 2012, vol. 90, no. 3, pp. 120–124.

37. Dong, Q., Santhanagopalan, S., and White, R.E., *J. Electrochem. Soc.*, 2008, vol. 155, no. 9, pp. B963–B968.

38. Dong, Q., Santhanagopalan, S., and White, R.E., *J. Electrochem. Soc.*, 2007, vol. 154, no. 8, pp. A816–A825.

39. Bird, R.B., Stewart, W.E., and Lightfoot, E.N., *Transport Phenomena*, 2nd Ed., New York: John Wiley & Sons, Inc., 2002.

40. Comsol Multiphysics, *Version 3.2*, Reference Manual, 2005.

41. Bower, V.E. and Davis, R.S., *J. Res. Nat. Bureau Standards*, 1980, vol. 85, no. 3, pp. 175–191.

42. Albery, W.J. and Bruckenstein, S., *Trans. Faraday Soc.,* 1966, vol. 62, pp. 1920–1924.

43. Markovic, N.M., Gasteiger, H.A. and Ross. P.N., Jr., *J. Phys. Chem.*, 1995, vol. 99, pp. 3411–3418.

44. Adanuvor, P.K., White, R.E., and Lorimer, S.E., *J. Electrochem. Soc.*, 1987, vol. 134, pp. 1450–1454.

45. Henstridge, M., Laborda, E., Rees, N.V., and Compton, R.G., *Electrochim. Acta*, 2012, vol. 84, pp. 12–20.